DRUG DEVELOPMENT AND INDUSTRIAL PHARMACY®
Vol. 30, No. 4, pp. 413–425, 2004

RESEARCH PAPER

The 3D Model: Explaining Densification and Deformation Mechanisms by Using 3D Parameter Plots

Katharina M. Picker*

Institute of Pharmaceutical Technology and Biopharmacy,
Martin-Luther-University Halle-Wittenberg, Halle/Saale, Germany

ABSTRACT

The aim of the study was to analyze very differently deforming materials using 3D parameter plots and consequently to gain deeper insights into the densification and deformation process described with the 3D model in order to define an ideal tableting excipient. The excipients used were dicalcium phosphate dihydrate (DCPD), sodium chloride (NaCl), microcrystalline cellulose (MCC), xylitol, mannitol, α-lactose monohydrate, maltose, hydroxypropyl methylcellulose (HPMC), sodium carboxymethylcellulose (NaCMC), cellulose acetate (CAC), maize starch, potato starch, pregelatinized starch, and maltodextrine. All of the materials were tableted to graded maximum relative densities ($\rho_{rel,\ max}$) using an eccentric tableting machine. The data which resulted, namely force, displacement, and time, were analyzed by the application of 3D modeling. Different particle size fractions of DCPD, CAC, and MCC were analyzed in addition. Brittle deforming materials such as DCPD exhibited a completely different 3D parameter plot, with low time plasticity, d, and low pressure plasticity, e, and a strong decrease in ω values when densification increased, in contrast to the plastically deforming MCC, which had much higher d, e, and ω values. e and ω values changed only slightly when densification increased for MCC. NaCl showed less of a decrease in ω values than DCPD did, and the d and e values were between those of MCC and DCPD. The sugar alcohols, xylitol and mannitol, behaved in a similar fashion to sodium chloride. This is also valid for the crystalline sugars, α-lactose monohydrate, and maltose. However, the sugars are more brittle than the sugar alcohols. The cellulose derivatives, HPMC, NaCMC, and CAC, are as plastic as MCC, however, their elasticity depends on substitution indicated by lower (more elastic) or higher (less elastic) ω values. The native starches, maize starch and potato starch, are very elastic, and pregelatinized starch and maltodextrine are less elastic and exhibited

*Correspondence: Katharina M. Picker, Institute of Pharmaceutical Technology and Biopharmacy, Martin-Luther-University Halle-Wittenberg, Wolfgang-Langenbeck-Str. 4, 06120 Halle/Saale, Germany; Fax: +49-345-552-7029; E-mail: picker@pharmazie.uni-halle.de.

DOI: 10.1081/DDC-120030936
0363-9045 (Print); 1520-5762 (Online)

higher ω values. Deformation behavior as shown in 3D parameter plots depends on particle size for polymers such as CAC and MCC; however, it does not depend on particle size for brittle materials such as DCPD. An ideally deforming tableting excipient should exhibit high e, d, and ω values with a constant ratio of e and ω at increasing densification.

Key Words: Tableting; Compaction; Excipients; 3D model; Particle size; Compression; Mathematical modeling.

INTRODUCTION

Tablets have been produced for more than 150 years, however, in order to describe the tableting process more precisely, tableting machines began to be instrumented for different purposes. In 1951, Brake[1] was the first to measure upper punch force, and shortly later Higuchi et al.[2,3] published similar results. In 1954/55[3,4] it became possible to measure upper punch displacement. These were the most relevant inventions concerning the analysis of the tableting process by means of mathematical modeling. With regard to both variables, force and displacement, a time dependent analysis can be done. Functional relationships referring to physical principles were set up derived from the data.[3–18] Most models used either force and displacement,[3–12] force and time,[13–16] or time and displacement.[17,18] Analysis of force and displacement can be divided into two groups: pressure/volume analysis[3–10] and force/displacement analysis.[11,12] The first group allows insights into the densification process, the second group is used to analyze compaction work. By means of force/time measurement a time dependent analysis was done on the plasto-elastic behavior of the materials. Only with the help of viscoelasticity models[19,20] can an interpretation be made of all of the values at the same time. However, when the data have to be fitted very precisely, these models become very complex and inconvenient. Therefore, the 3D modeling technique[21,22] was developed that enabled parameters to be derived, which can characterize tableting data and this in turn reveals densification and deformation behavior.

For a complete analysis of the process of tablet formation, in addition to the analysis of the tableting data always elastic recovery after tableting has to be analyzed. However, this is not the aim of this paper, which concentrates on 3D modeling.

Theoretical Background

To analyze the data gained during a single compaction cycle, namely force, time and displacement, these data were plotted in a 3D data plot (e.g., Fig. 1) as pressure (y), normalized time (x), and porosity according to Heckel (z).[6] On this 3D data plot, a twisted plane can be fitted by the least-squares method according to Levenberg–Marquard. The plane is twisted at $t=t_{max}$. The equation[a] is as follows:

$$z = \ln\left(\frac{1}{1-D_{rel}}\right) = ((t-t_{max})\cdot(d+\omega \cdot p_{max}-p)) + (e\cdot p) + (f + d\cdot t_{max}) \quad (1)$$

where D_{rel}=relative density, t=normalized time, p=pressure,

$$d = \frac{\delta \ln(1/(1-Drel))}{\delta t},$$

$$e = \frac{\delta \ln(1/(1-D_{rel}))}{\delta p},\ f = \ln\left(\frac{1}{1-D_0}\right)$$

where t_{max}=normalized time at maximum pressure, p_{max}=the maximum pressure, ω=twisting angle at t_{max}, and D_0=relative density at t=0.

For fitting, only those data exceeding a pressure of 50% of the maximum pressure were used. The percentage of 50% was chosen as a compromise between a minimum error of residues (0.0066 for 81 data sets) and the inclusion of as much data as possible. This procedure was regarded as legitimate, since the main particle deformation occurs during this stage and different stages of densification were included in further analyses.

[a]The equation is given in exact mathematical notation; in previous papers[21,22] the notation was given as used in MatLab®.

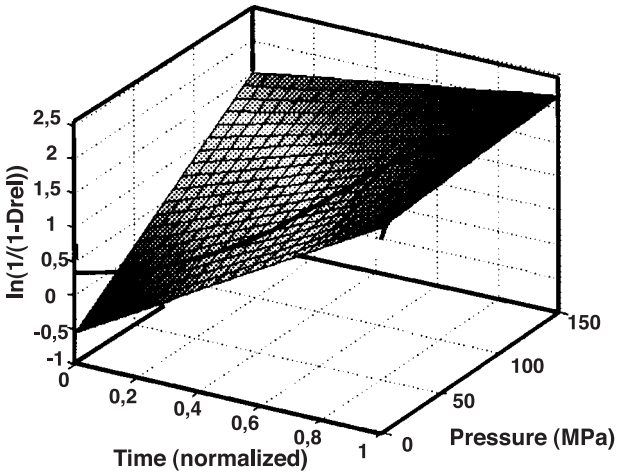

Figure 1. 3D data plot for one compaction cycle with a fitted twisted plane according to the 3D model.

From this fitting process different parameters can be calculated:[21,22] d, the slope of porosity over time called ''time plasticity,'' e, the slope of porosity over pressure called ''pressure plasticity,'' and ω, the twisting angle that indicates fast elastic decompression. f is the intersection of the untwisted plane with the z-axis (0, 0, f). This intersection at t=0 and p=0 is not directly correlated to the data between 50% and 100% of the maximum pressure and will thus be neglected in further interpretation. Materials that densify quickly show high d values and thus high time plasticity, and materials that densify easily and with low pressure show high e values and thus high pressure plasticity. Elastically deforming materials can demonstrate high decompression already during the tableting process. Consequently, the fitted plane is less twisted and the ω values are low. For each tableting condition, which means a certain maximum pressure or minimum porosity under load for a given weight of the tablet, a specific compaction cycle results that can be characterized by fitting the twisted plane. Specific d, e, and ω values can be calculated. By plotting the different characteristic parameters for each tableting excipient in a 3D coordinate system, a 3D parameter plot (e.g., Fig. 2) can be obtained, giving a simple yet characteristic description of the tableting properties.

Objective of the Study

The aim of this study is to use the parameters derived from 3D modeling in order to characterize very different materials using 3D parameter plots and to gain deeper insights into the densification and deformation process as described with the 3D model. Secondly, the aim is to derive which parameters are necessary for an ideally deforming tableting excipient.

EXPERIMENTAL

Materials

Dicalcium phosphate dihydrate (DCPD) (Emcompress®, lot #R 19 K, Mendell, Patterson, NJ), sodium chloride (NaCl) [pure (99.9%), lot #30940440, Roth Karlsruhe, Germany], and microcrystalline cellulose (MCC) (Avicel PH 102®, lot #7808C, FMC, Princeton, NJ) were used as materials with strongly different deformation mechanisms. Two different sugar alcohols, xylitol granulated with sodium carboxymethylcellulose (Xylitab 200®, lot #332013 P, Xyrofin Oy Kotka, Finland) and granulated mannitol (Pearlitol SD 200®, lot #69-65-8, Roquettes Frères, Lestrem, France), as well as two different sugars, α-lactose monohydrate (SpheroLac 100®, lot #S0046, Meggle GmbH, Wasserburg, Germany) and crystalline maltose (Advantose 100®, lot #970223, SPI Polyols, New Castle, DE) were analyzed. Different cellulose derivatives, hydroxypropyl methylcellulose (HPMC) (Metolose 90 SH 15.000®, lot #506825, Shin-Etsu, Tokyo, Japan), sodium carboxymethylcellulose (NaCMC) (3000 cP, lot #16110, Serva Feinbiochemica, Heidelberg, Deutschland), and cellulose acetate (CAC) (CA 398-10®, lot #AC-632505, Eastman Chemical Company, Kingsport, TN) were compared to MCC. Different

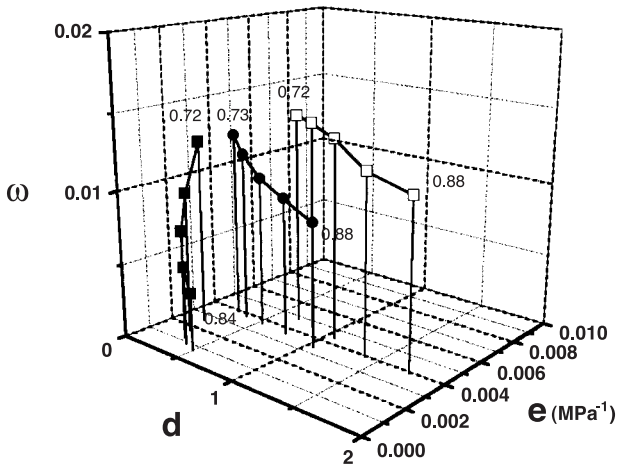

Figure 2. 3D parameter plot of ■ DCPD, □ MCC, and ● NaCl at different $\rho_{rel,\ max}$ (means of n=5).

starches and starch derivatives, maize starch (lot #43183255) and potato starch (lot #35439.008E5) according to Pharmacopoea Europea (Wasserfuhr GmbH, Bonn, Germany), a pregelatinized starch (Starch 1500®, lot #606009, Colorcon West Point, PA), and maltodextrine (Glucidex 19®, lot #9050-36-6, Roquettes Frères, Lestrem, France) were characterized as well.

Methods

Particle Size Determination and Preparation of Sieve Fractions

Particle size distribution was determined by sieve analysis according to DIN 66165 (Retsch sieving machine, Type Vibrio, No. 12189031, Retsch GmbH und Co. KG, Haan, Germany). In cases where the particles were too small, laser light diffractometry using a dry feeder (Sympatec Rodos, Type 12SR, pressure 3.5 bar, injection pressure 85 to 90 mbar) was applied. The median of the particle size distribution was determined at 50%.

For DCPD, CAC, and MCC, four different sieve fractions were prepared using a set of sieves with different mesh sizes on a vibrating sieving machine (Retsch sieving machine, Type Vibrio). The sieve sizes were chosen according to the desired particle size fractions. The following particle size fractions were prepared: 0–90, 90–125, 125–180 and >180 μm.

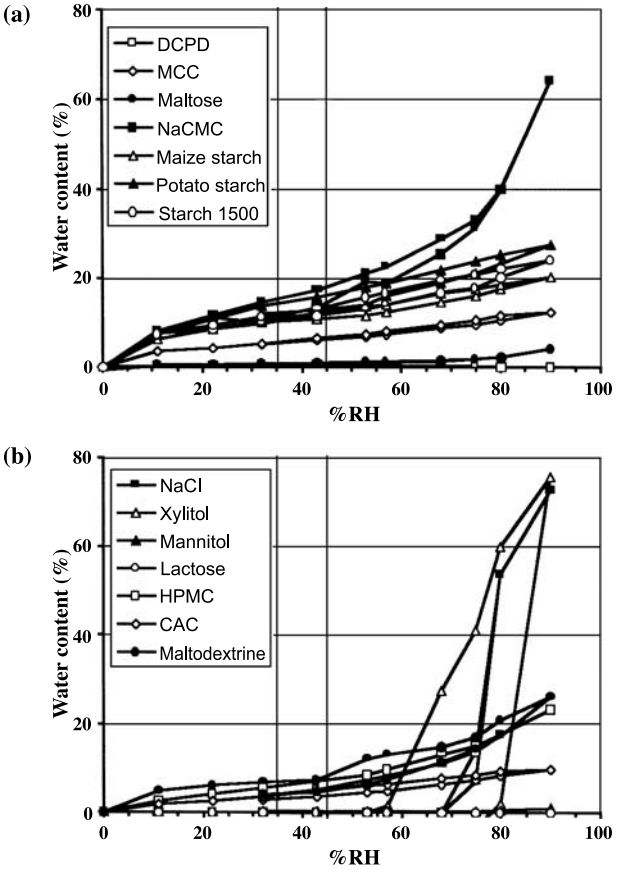

Figure 3. Sorption and desorption isotherms of the excipients used (means of n=2).

Test Conditions

All of the experiments were performed at a relative humidity (RH) between 35% and 45%. Tableting was performed in a special climate controlled room, which was set to 23±1°C and 45±2% RH. Under these conditions neither sorption nor desorption had an effect on the experiments. To ensure this, the water content of the materials being used for tableting was determined by thermogravimetric analysis in triplicate (data not shown) (TG, Netzsch Gerätebau, Selb, Germany), and sorption isotherms were recorded gravimetrically after equilibration over saturated salt solutions in duplicate (Fig. 3). Means were calculated. The water content correlated with the sorption isotherms. In addition, the isotherms indicated that the water sorption/desorption was marginal, in the range between 35% and 45% RH.

True Density

The true density (ρ_{true}) of all of the materials was determined by Helium pycnometry (Accupyc 1330, Micromeritics, Norcross, GA) in triplicate. Under the conditions given above, this ''true'' density is equal to the apparent particle density.

Tableting

Tableting was performed on an instrumented single punch tableting machine (EK0/DMS, No. 1.0083.92, Korsch GmbH, Berlin, Germany) with 11-mm-diameter flat-faced punches (Ritter GmbH, Hamburg, Germany). Equal true volumes of the substances were tableted to five different maximum relative densities ($\rho_{rel,\ max}$) of the tablets (precision 0.001). The selected $\rho_{rel,\ max}$ are given in Tables 1–5. $\rho_{rel,\ max}$ is defined as follows:

$$\rho_{rel,\ \max} = \frac{\rho_{\max}}{\rho_{true}} \qquad (2)$$

Table 1. Calculated means and standard deviations for the parameters of 3D modeling for dicalcium phosphate dihydrate, sodium chloride, and microcrystalline cellulose.

Materials	Medium particle size (μm)	$\rho_{rel,\ max}$	d	e (MPa^{-1})	ω
Dicalcium phosphate dihydrate	145	0.84	0.4978 ± 0.0076	0.0007 ± 0.0000	0.0039 ± 0.0002
		0.82	0.3933 ± 0.0033	0.0009 ± 0.0000	0.0053 ± 0.0001
		0.79	0.3123 ± 0.0066	0.0012 ± 0.0000	0.0074 ± 0.0002
		0.76	0.2510 ± 0.0101	0.0017 ± 0.0001	0.0096 ± 0.0006
		0.72	0.1933 ± 0.0135	0.0026 ± 0.0001	0.0126 ± 0.0010
Sodium chloride	145	0.88	1.0516 ± 0.0048	0.0034 ± 0.0000	0.0085 ± 0.0001
		0.85	0.7666 ± 0.0027	0.0036 ± 0.0001	0.0094 ± 0.0002
		0.81	0.5358 ± 0.0017	0.0037 ± 0.0001	0.0103 ± 0.0001
		0.77	0.3625 ± 0.0018	0.0038 ± 0.0001	0.0116 ± 0.0002
		0.73	0.2609 ± 0.0018	0.0039 ± 0.0001	0.0127 ± 0.0002
Microcrystalline cellulose	75	0.88	1.7585 ± 0.0105	0.0039 ± 0.0001	0.0115 ± 0.0002
		0.84	1.3718 ± 0.0165	0.0041 ± 0.0001	0.0121 ± 0.0002
		0.80	1.0626 ± 0.0215	0.0045 ± 0.0001	0.0144 ± 0.0005
		0.76	0.8444 ± 0.0033	0.0046 ± 0.0001	0.0142 ± 0.0002
		0.72	0.6693 ± 0.0015	0.0048 ± 0.0001	0.0141 ± 0.0002

with $\rho_{rel,\ max}$ = maximum relative density, ρ_{max} = density at minimum height of the tablet under load, and ρ_{true} = true density.

The tablet height at maximum densification under load was held constant at 3 mm. Displacement of the punch faces was measured using an inductive transducer (W20 TK, Hottinger Baldwin Meßtechnik, Darmstadt, Germany) and corrected for elastic deformation of the punches. The depth of filling was held constant at 13 mm. The machine speed was set to 10

Table 2. Calculated means and standard deviations for the parameters of 3D modeling for the sugars and sugar alcohols.

Materials	Medium particle size (μm)	$\rho_{rel,\ max}$	d	e (MPa^{-1})	ω
Xylitol	165	0.88	1.3907 ± 0.0192	0.0032 ± 0.0001	0.0071 ± 0.0002
		0.84	1.0930 ± 0.0560	0.0034 ± 0.0001	0.0090 ± 0.0004
		0.81	0.7850 ± 0.0444	0.0039 ± 0.0001	0.0111 ± 0.0006
		0.77	0.3636 ± 0.0120	0.0050 ± 0.0001	0.0126 ± 0.0010
		0.72	0.2440 ± 0.0113	0.0066 ± 0.0002	0.0154 ± 0.0006
Mannitol	150	0.88	1.2692 ± 0.0522	0.0030 ± 0.0001	0.0075 ± 0.0004
		0.84	0.9497 ± 0.0433	0.0031 ± 0.0001	0.0100 ± 0.0005
		0.81	0.7258 ± 0.0060	0.0036 ± 0.0001	0.0136 ± 0.0002
		0.77	0.6234 ± 0.0795	0.0040 ± 0.0002	0.0175 ± 0.0007
		0.72	0.4852 ± 0.1064	0.0046 ± 0.0007	0.0226 ± 0.0040
Maltose	135	0.88	1.4104 ± 0.0081	0.0030 ± 0.0001	0.0040 ± 0.0002
		0.85	0.8961 ± 0.0303	0.0030 ± 0.0002	0.0063 ± 0.0004
		0.81	0.6114 ± 0.0089	0.0031 ± 0.0002	0.0082 ± 0.0004
		0.77	0.4321 ± 0.0150	0.0039 ± 0.0002	0.0100 ± 0.0004
		0.73	0.3239 ± 0.0047	0.0040 ± 0.0001	0.0113 ± 0.0003
α-lactose monohydrate	100	0.88	0.8055 ± 0.0048	0.0037 ± 0.0001	0.0063 ± 0.0000
		0.85	0.5934 ± 0.0034	0.0039 ± 0.0001	0.0085 ± 0.0001
		0.81	0.4483 ± 0.0188	0.0048 ± 0.0001	0.0117 ± 0.0007
		0.77	0.3236 ± 0.0022	0.0057 ± 0.0002	0.0144 ± 0.0004
		0.73	0.2419 ± 0.0011	0.0071 ± 0.0002	0.0177 ± 0.0005

Table 3. Calculated means and standard deviations for the parameters of 3D modeling for the cellulose derivatives.

Materials	Medium particle size (μm)	$\rho_{rel,\ max}$	d	e (MPa^{-1})	ω
HPMC	45	0.90	1.3958±0.0511	0.0065±0.0001	0.0113±0.0005
		0.86	1.0899±0.0072	0.0067±0.0001	0.0150±0.0002
		0.82	0.8085±0.0031	0.0073±0.0001	0.0167±0.0003
		0.78	0.5995±0.0037	0.0081±0.0001	0.0191±0.0001
		0.73	0.5262±0.0022	0.0106±0.0002	0.0291±0.0005
NaCMC	45	0.87	1.2347±0.0293	0.0034±0.0000	0.0005±0.0000
		0.83	0.9622±0.0509	0.0033±0.0002	0.0016±0.0003
		0.80	0.6730±0.0218	0.0034±0.0002	0.0028±0.0007
		0.76	0.4914±0.0535	0.0033±0.0000	0.0036±0.0004
		0.72	0.3230±0.0055	0.0034±0.0001	0.0046±0.0000
Cellulose acetate	160	0.89	2.0427±0.0594	0.0056±0.0000	0.0041±0.0003
		0.85	1.5316±0.0516	0.0056±0.0004	0.0060±0.0002
		0.81	1.2318±0.0229	0.0059±0.0001	0.0065±0.0001
		0.77	0.9797±0.0332	0.0062±0.0001	0.0071±0.0002
		0.72	0.7800±0.0341	0.0066±0.0002	0.0072±0.0007

revolutions per minute. Lubricant (0.5% w/w magnesium stearate) was only used for DCPD and α-lactose monohydrate. No lubrication was used with the other materials in order to avoid it having any effect on the microstructure of the tablet. The amount of material necessary for each tablet with a given $\rho_{rel,\ max}$ and the same apparent density was calculated. The powder was manually filled into the die. One compaction cycle was performed and five single tablets were produced for each individual condition.

Calibration of the Force and Displacement Transducers

The strain gauges were calibrated quasistatically with two load cells of different working ranges (0–10 kN, type C2, #00842 and 10–50 kN, type C2, #81499, Spectris Messtechnik, Langen, Germany). The load cells were fixed with a special mounting (University Halle-Wittenberg) instead of the upper punch. Upper punch force, lower punch force, and reference force

Table 4. Calculated means and standard deviations for the parameters of 3D modeling for the starches and starch derivatives.

Materials	Medium particle size (μm)	$\rho_{rel,\ max}$	d	e (MPa^{-1})	ω
Maize starch	<20	0.89	1.7211±0.0446	0.0059±0.0002	0.0019±0.0005
		0.85	1.2285±0.0060	0.0059±0.0001	0.0029±0.0001
Potato starch	30	0.89	1.4607±0.0020	0.0057±0.0001	0.0048±0.0002
		0.85	0.9884±0.0086	0.0062±0.0001	0.0061±0.0002
		0.82	0.6766±0.0027	0.0067±0.0001	0.0063±0.0001
Pregelatinized starch	75	0.88	1.5094±0.0114	0.0045±0.0001	0.0063±0.0001
		0.85	1.0653±0.0086	0.0046±0.0001	0.0071±0.0002
		0.81	0.7566±0.0227	0.0047±0.0000	0.0085±0.0003
		0.77	0.5240±0.0042	0.0049±0.0001	0.0091±0.0000
		0.73	0.3714±0.0015	0.0053±0.0001	0.0104±0.0003
Maltodextrine	95	0.88	1.7670±0.0391	0.0049±0.0000	0.0032±0.0004
		0.85	1.1593±0.0174	0.0032±0.0001	0.0074±0.0003
		0.81	0.7136±0.0091	0.0039±0.0001	0.0070±0.0004
		0.77	0.4900±0.0089	0.0035±0.0001	0.0086±0.0002
		0.73	0.2639±0.0034	0.0050±0.0002	0.0130±0.0003

Table 5. Calculated means and standard deviations for the parameters of 3D modeling for various particle size fractions of different excipient.

Materials	Particle size (μm)	$\rho_{rel,\ max}$	d	e (MPa^{-1})	ω
Dicalcium phosphate dihydrate	<90	0.84	0.3433±0.0031	0.0016±0.0000	0.0028±0.0000
		0.78	0.2444±0.0013	0.0016±0.0000	0.0051±0.0000
		0.72	0.1664±0.0007	0.0021±0.0001	0.0090±0.0000
	90–125	0.84	0.5077±0.0039	0.0012±0.0000	0.0032 ±0.0001
		0.78	0.3120±0.0027	0.0016±0.0000	0.0058±0.0000
		0.72	0.2003±0.0015	0.0024±0.0000	0.0117±0.0003
	125–180	0.84	0.3783±0.0012	0.0016±0.0000	0.0035±0.0003
		0.78	0.2463±0.0017	0.0016±0.0000	0.0063±0.0000
		0.72	0.1715±0.0004	0.0023±0.0001	0.0119±0.0001
	>180	0.84	0.5177±0.0018	0.0014±0.0000	0.0034±0.0001
		0.78	0.3296±0.0012	0.0018±0.0000	0.0069±0.0001
		0.72	0.2137±0.0074	0.0027±0.0001	0.0141±0.0005
Cellulose acetate	<90	0.89	1.7142±0.0368	0.0037±0.0001	0.0077±0.0001
		0.81	1.1405±0.0505	0.0048±0.0000	0.0091±0.0004
		0.72	0.6840±0.0060	0.0052±0.0000	0.0109±0.0002
	90–125	0.89	1.9608±0.0220	0.0037±0.0000	0.0086±0.0001
		0.81	1.2736±0.0098	0.0049±0.0001	0.0100±0.0001
		0.72	0.8149±0.0329	0.0054±0.0001	0.0120±0.0005
	125–180	0.89	2.2713±0.0334	0.0045±0.0001	0.0066±0.0002
		0.81	1.4010±0.0050	0.0048±0.0000	0.0099±0.0000
		0.72	0.8602±0.0054	0.0053±0.0001	0.0115±0.0001
	>180	0.89	2.3717±0.1006	0.0056±0.0003	0.0041±0.0009
		0.81	1.3817±0.0033	0.0047±0.0000	0.0094±0.0001
		0.72	0.8632±0.0025	0.0054±0.0001	0.0106±0.0002
Microcrystalline cellulose	<90	0.88	1.6441±0.0337	0.0027±0.0000	0.0113±0.0004
		0.80	1.0392±0.0592	0.0033±0.0001	0.0123±0.0007
		0.72	0.6678±0.0030	0.0040±0.0000	0.0139±0.0002
	90–125	0.88	1.6782±0.0669	0.0026±0.0001	0.0119±0.0004
		0.80	1.0872±0.0729	0.0033±0.0000	0.0131±0.0008
		0.72	0.7449±0.0399	0.0041±0.0000	0.0157±0.0007
	125–180	0.88	1.6800±0.0139	0.0027±0.0000	0.0121±0.0003
		0.80	1.1867±0.0434	0.0034±0.0002	0.0145±0.0007
		0.72	0.7823±0.0094	0.0041±0.0000	0.0168±0.0002
	>180	0.88	1.3832±0.3087	0.0027±0.0001	0.0115±0.0022
		0.80	1.2133±0.0356	0.0034±0.0002	0.0148±0.0007
		0.72	0.8046±0.0085	0.0041±0.0001	0.0171±0.0003

were measured after repeated preloading on three different days. The reference forces increased with an increment of 0.5 kN up to 5 kN, and they increased with an increment of 2.5 kN up to 32.5 kN. Each measurement was repeated twice. With regard to all of the data obtained for upper and lower strain gauge, a calibration function was set up using linear regression. The determination coefficient was better than 0.9999. While using the same procedure, the calibration was verified by calibrating the upper punch against the lower punch.

The inductive displacement transducer was calibrated with round-shaped slip gauges of defined height (2–6 mm, precision 0.001, University Halle-Wittenberg) and a diameter of 10.98 mm in the die. In this way the tablet height could be directly determined in the die. The measured height was corrected for elastic punch and machine deformation. Total elastic deformation was analyzed using punch-to-punch pressings. Elastic deformation of the upper punch was determined separately by pressing the upper punch against a 200-mm-high hardened stainless steel plate (quality

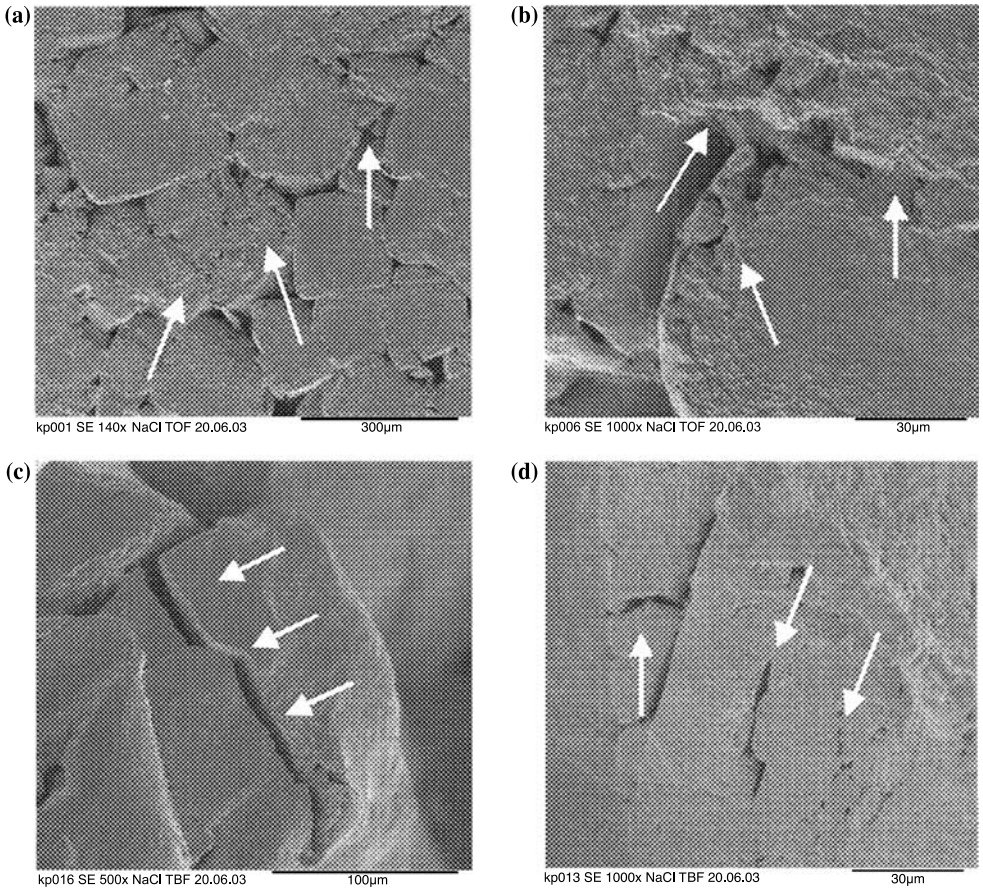

Figure 4. SEMs of NaCl tablets: (a) surface (magnification 140×), (b) surface (magnification 1000×), (c) interior (fractured surface) (magnification 500×), and (d) interior (magnification 1000×).

1.4112, Ritter GmbH, Hamburg). Since this measurement can be influenced by the elastic deformation of the steel plate, the elastic deformation of the steel plate was also determined using the difference established between the elastic deformation with and without steel plate. This value could be subtracted from the upper punch elastic deformation, and by this means the elastic deformation of upper punch and upper punch holder was determined. The lower punch elastic deformation was calculated from the difference between the total and the upper punch elastic deformation. The total elastic deformation was 11.5 µm kN^{-1}, the upper punch elastic deformation was 7.9 µm kN^{-1} and the lower punch elastic deformation was 3.9 µm kN^{-1}. Since the elastic deformation was in accordance with Hooke's law, displacement was corrected by adding the elastic deformation to the tablet height according to the measured force.

Data Acquisition

Data acquisition was performed by a DMC-plus system (Hottinger Baldwin Meßtechnik, Darmstadt, Germany), and the data were stored by BEAM-Software (AMS-Flöha, Germany). The 3D modeling method was applied using Matlab® (The Mathworks, Unterföhring, Germany). The resulting parameters d, e, and ω of the five compaction cycles for each tableting condition (material, a given $\rho_{rel,\ max}$ and/or particle size fraction) were averaged and the means and standard deviations were calculated (Tables 1–5).

Scanning Electron Microscopy

Broken tablets were mounted onto a sample holder and coated with coal/gold/coal. The samples were examined with a scanning electron microscope (SEM)

(model JSM 6400, Jeol, Tokyo, Japan) at an accelerating voltage of 15 or 5 kV depending on the sample.

RESULTS AND DISCUSSION

Figure 2 (Table 1) shows the deformation behavior of very differently deforming substances as MCC, NaCl, and DCPD. Microcrystalline cellulose exhibited high d values, which rose with increasing densification. The e values were medium and decreased slightly with increasing $\rho_{rel,\ max}$.[b] This means that MCC exhibited high time plasticity and medium pressure plasticity, which decreased with increasing $\rho_{rel,\ max}$. Simultaneously, ω decreased slightly, and therefore there was an increase in fast elastic decompression. This indicates viscoelasticity; however, it must be noted that ω is in the middle range, which presents more plasticity than elasticity.

Dicalcium phosphate dihydrate displayed a completely different deformation behavior. The d and e values were low, even when $\rho_{rel,\ max}$ increased. This means that the material is not plastically deforming; it requires time and high pressure for deformation. In addition, whether or not the material is brittle or elastically deforming can be established. At low $\rho_{rel,\ max}$, ω is high and thus fast elastic decompression is low; at higher $\rho_{rel,\ max}$, ω decreases and the deformation is more elastic, even when d and e do not change a great deal. This change from low relaxation to high relaxation at similar pressure plasticity indicates brittleness. When particles break, new smaller particles are formed. These particles deform again, however, and when there are fewer defects, they deform more elastically.

NaCl behavior lies between that of MCC and DCPD; even when it is described in the literature as a plastically deforming excipient.[23–25] It exhibits lower time plasticity, d, and lower pressure plasticity, e, than MCC, however much more than with regard to DCPD. It is important that its pressure plasticity does not decrease as it does with MCC. This means that the plasticity described in the literature is mainly pressure plasticity, which is expressed in permanent deformation. It must also be mentioned that ω is lower, and the decrease that occurs when d increases, is higher here than for MCC. So we may conclude that NaCl also deforms slightly by fracture, but fast elastic decompression is much lower for NaCl than for DCPD, since ω is higher. These results can be underlined analyzing SEMs of NaCl tablets (Fig. 4a–d). Small cracks and slight fractures are visible.

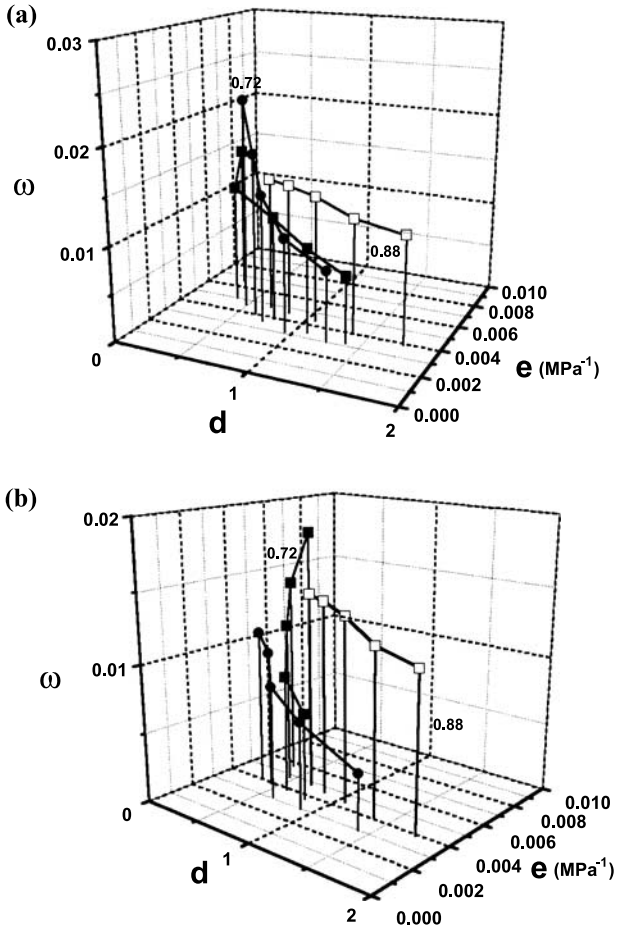

Figure 5. 3D parameter plot of (a) ■ xylitol, ● mannitol, and □ MCC, and (b) ■ α-lactose monohydrate, ● maltose, and □ MCC (means of n=5).

Figure 5a (Table 2) shows two examples for sugar alcohols, xylitol and mannitol. These materials displayed similarities to NaCl (lower time and pressure plasticity) when compared to MCC. Nevertheless, their time plasticity is higher than that of NaCl. When densification increases, ω values and e values strongly decrease. This indicates brittleness as in the case of DCPD. Furthermore, at low densification ω is high and therefore fast elastic decompression is low. The results

[b]In the previously published paper,[21] a calculation error influenced the results and influenced particularly e value tendencies (increasing with $\rho_{rel,\ max}$ in Ref. [21] and decreasing here). This has been corrected and the correct data are now given in this paper.

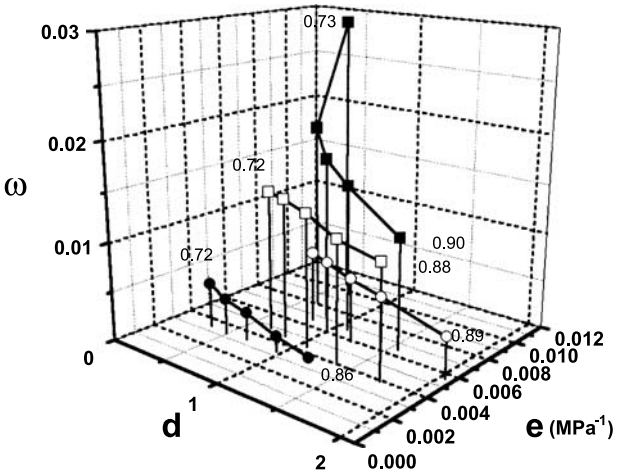

Figure 6. 3D parameter plot of ■ HPMC, ○ CAC, ● NaCMC, and □ MCC (means of n=5).

are in accordance with those found in the literature. Brittle fracture was described for xylitol[26] and mannitol.[27] It is more pronounced for xylitol than for mannitol. This clearly indicates a difference in material, since the medium particle size and the particle size distributions of both materials are similar. In this study the sugars α-lactose monohydrate and maltose were analyzed by 3D modeling (Fig. 5b, Table 2). α-lactose monohydrate exhibited lower pressure plasticity, e, than MCC at the highest $\rho_{rel,\ max}$. Maltose exhibited lower pressure plasticity, e, than MCC at all $\rho_{rel,\ max}$. Furthermore, e decreases simultaneously to ω, indicating that these materials are brittle, however, less brittle than DCPD. This was more pronounced for α-lactose monohydrate and this material also showed the lowest time plasticity out of all of the sugars and sugar alcohols. In the literature α-lactose monohydrate is described as brittle with low amounts of plastic deformation.[28,29] However, its pressure plasticity is much higher than that of DCPD. Maltose shows with regard to all $\rho_{rel,\ max}$ lower d, e, and ω values than MCC. Its densification ability is lower than the densification ability of MCC. The decrease in pressure plasticity is higher than for MCC, and fast elastic decompression is also higher than for MCC. On the whole, tableting behavior as described in the literature is acceptable, and this behavior consists partially of brittle fracture and sufficient plastic deformation.

Figure 6 (Table 3) shows the deformation behavior of different cellulose derivatives. The deformation characteristics characterized by 3D modeling are different when compared to those of MCC. Whereas HPMC shows higher pressure plasticity, e, and less relaxation, which is indicated by higher ω values, NaCMC and CAC show very low ω values. For NaCMC pressure plasticity is also lower. Time plasticity for HPMC and for NaCMC is lower than for MCC, and it is higher for CAC than for MCC. The results are similar when they are compared to those of earlier studies done on HPMC and NaCMC[30] and CAC,[22] where the materials were analyzed by Heckel plots, elastic recovery measurements, and pressure time plots. In previous studies it was shown that the degree of polymerization has no relevance since no evidence was detected that compaction properties are influenced.[30] Therefore, the difference in degree of polymerization does not influence the interpretation of the results.

Starch is a very elastic material. In Fig. 7a and b (Table 4), the deformation behavior of different native starches, such as pregelatinized starch and the starch

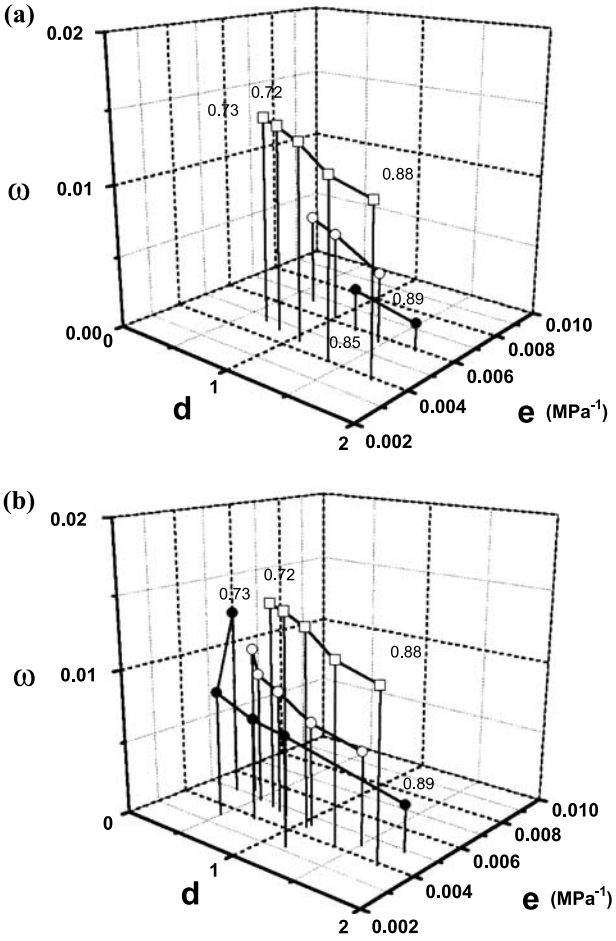

Figure 7. 3D parameter plot of (a) ● maize starch, ○ potato starch, and □ MCC, and (b) ● maltodextrine, ○ pregelatinized starch, and □ MCC (means of n=5).

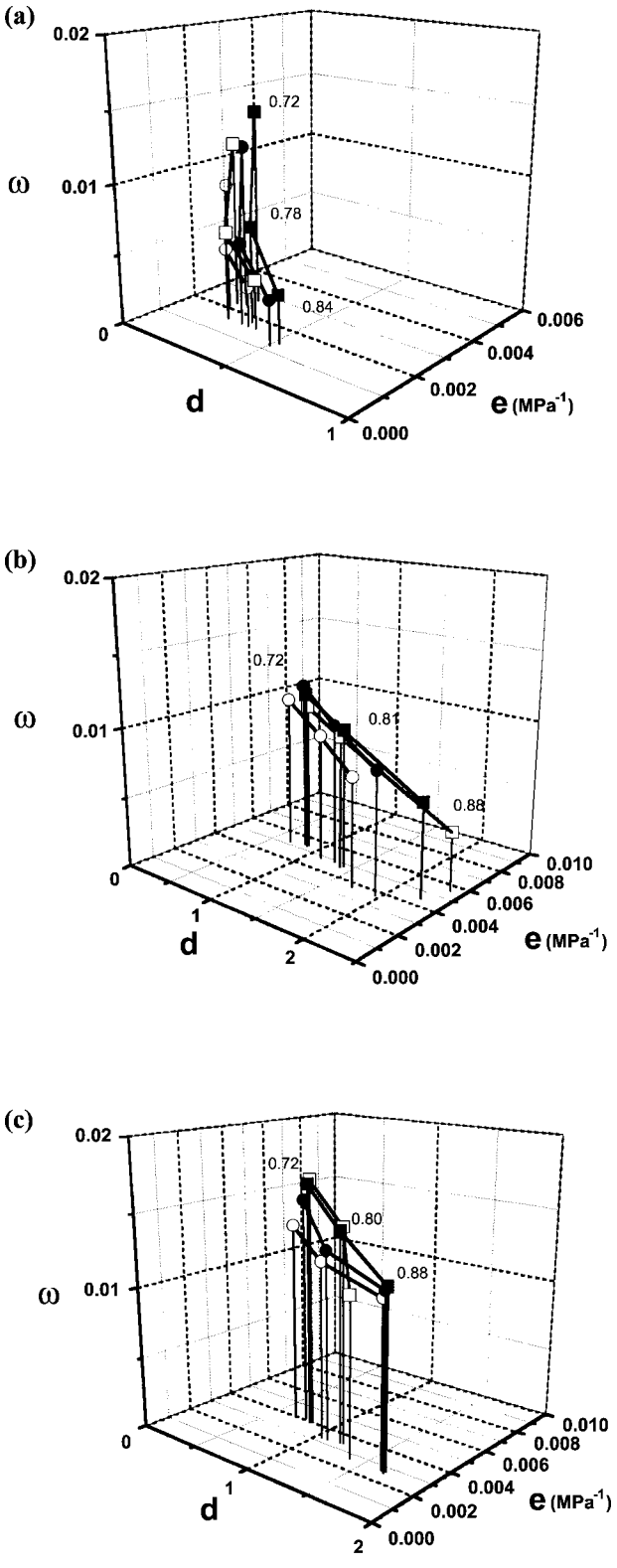

Figure 8. 3D parameter plot of different particle size fractions of (a) DCPD, (b) CAC, and (c) MCC: ○ < 90 μm, ● 90–125 μm, ■ 125–185 μm, and □ > 180 μm (means of n = 5).

hydrolysate maltodextrine is shown. The native starches maize and potato (Fig. 7a) exhibit a higher pressure plasticity, e, and a much higher fast elastic decompression than MCC, since ω is lower. Tablets were formed only at higher $\rho_{rel,\ max}$. It is generally known that their compactibility is poor.[31,32] Pregelatinized starch (Fig. 7b) could be tableted at all $\rho_{rel,\ max}$: ω decreased when densification increased. Its e values and therefore the pressure plasticity are comparable to MCC, but the fast elastic decompression is higher.

Maltodextrine, a starch hydrolysate, has lower e values when compared with the other starches. The d values strongly increased and its fast elastic decompression is comparable to that of pregelatinized starch at higher $\rho_{rel,\ max}$. At lower $\rho_{rel,\ max}$, with increasing $\rho_{rel,\ max}$, the e and ω values decreased and this indicated brittleness. Therefore, it is safe to say that this material deforms slowly, exhibits brittle and plastic deformation, and can therefore form better tablets than the native starches. Other authors[33,34] have already published statements regarding the acceptability of maltodextrine as a tableting excipient.

Lastly, different particle size fractions were analyzed, since tableting behavior is not only dependent on material properties but on differences in particle size as well. Therefore, it is also of utmost importance that particle size is always considered.

Figure 8a (Table 5) indicates the influence of particle size on the different particle size fractions of DCPD. Concerning this brittle material the particle size has little influence. The differences lie within the bounds of experimental error, even when not all of them fall within the limits of standard deviation. A small influence can be seen for ω at low $\rho_{rel,\ max}$, which indicates that the larger crystals exhibit more brittle fraction. In Fig. 8b (Table 5), the influence of particle size on the plastically deformable CAC can be seen. With regard to increasing particle size, time plasticity, d, especially increases at higher densification and pressure plasticity, e, increases slightly. This behavior is based on the fact that larger particles are more easily deformed and therefore they need less time for densification. Simultaneously, ω decreased at higher $\rho_{rel,\ max}$, and so fast elastic decompression increased. Here the influence of particle size is clearly visible. The influence of particle size is less with regard to MCC than it is for CAC, however, it is still visible. No influence on pressure plasticity was revealed. At first when particle size increases, ω increases since fast elastic decompression is lower. However, when the particles are still big they deform a little slower, and at this point d decreases. This behavior is only visible at the highest densification

and it almost falls within the limits of standard deviation. Overall, how the influence of particle size becomes visible depends on the nature of the material. The results are in accordance with the literature.[35] Concerning brittle materials such as DCPD, the influence of particle size was small and nearly always within the bounds of experimental error. Moreover, the deformation behavior of plastically deforming materials clearly changed.

CONCLUSIONS

The results show that differently deforming materials can be easily and precisely analyzed by employing 3D modeling. A simple description of the processes during tableting is possible, and thus densification and deformation properties can be clearly distinguished with a single model. It is no longer necessary to use two or more methods. The influence of pressure and time is analyzed in one step and further fast elastic decompression can be interpreted. Consequently, it is possible to interpret deformation and relaxation during tableting as essential mechanisms of the tablet formation process. For brittle deforming materials, d and e values are low, and the e values decrease when $\rho_{rel,\ max}$ increases. Simultaneously, there is a strong decrease in ω. Regarding materials such as DCPD, α-lactose monohydrate, and maltose, a dependence on true density is visible. The higher the density and the strength of a material results in a lower ω and a higher fast elastic decompression. α-lactose monohydrate is the most ''plastic'' and consequently the most deformable material of these brittle materials. The higher the d and e values, the more easily deformable is a material.

However, when a material is viscoelastic, the d values increase strongly and the e values decrease slightly as $\rho_{rel,\ max}$ increases. Furthermore, the ω values only decrease if fast elastic decompression increases with increasing $\rho_{rel,\ max}$. An example of constant fast elastic decompression at all $\rho_{rel,\ max}$ is MCC. On the contrary, native starches have such a high amount of elasticity that they are only able to form tablets at higher densification taking into account the given experimental conditions.

We can interpret this to mean that the 3D modeling technique allows one to differentiate among brittle fracture, plastic deformation, elastic relaxation, and viscoelasticity.

When comparing the 3D modeling technique with other methods, the main advantage compared to the Heckel-in-die-method is that elastic decompression is eliminated directly during calculation at the best. Furthermore, in addition to the interpretation of a pressure-porosity plot the time influence has been interpreted.

The question still remains as to which combination of the 3D modeling parameters should an ideal tableting excipient have, an excipient which possesses a high proportion of plastic deformation and good bonding properties. Even when the data presented here were only obtained from compaction cycles derived from one tableting machine and the experimental conditions have influenced the absolute values, some general conclusions can of course be drawn.

When considering MCC, it is remarkable that the e and ω values stayed on the same level and only d increased. If e and ω remain in the same ratio, this means that there is a constant ratio of pressure plasticity and fast elastic decompression. Since deformation and relaxation are essential mechanisms of the tablet formation process, this means that tablet formation is similar for all of the different $\rho_{rel,\ max}$. Therefore, a goal should be to find a substance that is characterized by such a ratio of the parameters. Ideally, in the long run high time and pressure plasticity should be present in order to produce stable and robust tablets.

ACKNOWLEDGMENTS

The author thanks the companies mentioned in the materials section of this paper for donating the materials.

REFERENCES

1. Brake, E.F. Development of methods for measuring pressures during tablet manufacture. M.S. Thesis; Purdue University, 1951.
2. Higuchi, T.; Arnold, R.D.; Tucker, S.J.; Busse, L.W. The physics of tablet compression. I. A preliminary report. J. Am. Pharm. Assoc. **1952**, *41*, 93–96.
3. Higuchi, T.; Nelson, E.; Busse, L.W. The physics of tablet compression III: design and construction of an instrumented tableting machine. J. Am. Pharm. Assoc. **1954**, *43*, 344–348.
4. Nelson, E.; Busse, L.W.; Higuchi, T. The physics of tablet compression: VII. Determination of energy expenditure in the tablet compression process. J. Am. Pharm. Assoc. (Sci. Ed.) **1955**, *44*, 223.
5. Heckel, R.W. An analysis of powder compaction phenomena. Trans. Metall. Soc. AIME **1961**, *221*, 1001–1008.
6. Heckel, R.W. Density-pressure relationships in powder compaction. Trans. Metall. Soc. AIME **1961**, *221*, 671–675.

7. Kawakita, K.; Lüdde, K.H. Some considerations on powder compression equations. Powder Technol. **1970/71**, *4*, 61–68.
8. Cooper, A.R.; Eaton, L.E. Compaction behaviour of several ceramic powders. J. Am. Ceram. Soc. **1962**, *5*, 97–101.
9. Walker, E. The properties of powders. Part VII. The influence of the velocity of compression on the apparent compressibility of powders. Trans. Faraday Soc. **1923**, *19*, 614–620.
10. Bal'shin, M.Y. Contribution to the theory of powder metallurgical processes. Metalloprom. **1938**, *18*, 124–147.
11. Führer, C. Über den Druckverlauf bei der Tablettierung in Exzenterpressen. Dtsch. Apoth.-Ztg. **1962**, *102*, 827–842.
12. Moldenhauer, H.; Hühnerbein, B.; Kala, H. Recording of pressure-path diagrams from an eccentric press using piezoelectric measurement. Pharmazie **1972**, *27*, 417–418.
13. Emschermann, B.; Müller, F. Evaluation of force measurements in tablet manufacture. Pharm. Ind. **1981**, *43*, 191–194.
14. Schmidt, P.C.; Vogel, P.J. Force-time-curves of a modern rotary tablet machine. Part 1. Evaluation techniques and characterization of deformation behavior of pharmaceutical substances. Drug Dev. Ind. Pharm. **1994**, *20*, 921–934.
15. Dietrich, R.; Mielck, J.B. Parametrisierung des zeitlichen Verlaufs der Verdichtung bei der Tablettierung mit Hilfe der modifizierten Weibull-Funktion. Pharm. Ind. **1985**, *47*, 216–220.
16. Shlieout, G.; Wiese, M.; Zessin, G. A new method to evaluate the consolidation behavior of pharmaceutical materials by using the Fraser–Suzuki function. Drug Dev. Ind. Pharm. **1999**, *25*, 29–36.
17. Ho, A.Y.K.; Jones, T.M. Rise time: a new index of tablet compression. J. Pharm. Pharmacol. **1988**, *40*, 74P.
18. Tsardaka, E.D. Viscoelastic properties and compaction behavior of pharmaceutical particulate material. Ph.D. Thesis; University of Bath, 1990.
19. Müller, F.; Caspar, U. Viskoelastische Phänomene während der Tablettierung. Pharm. Ind. **1984**, *46*, 1049–1056.
20. Müller, F. Viscoelastic models. In *Pharmaceutical Powder Compaction Technology*; Alderborn, G., Nyström, C., Eds.; Marcel Dekker Inc.: New York, 1996; 99–132.
21. Picker, K.M. A new theoretical model to characterize the densification behavior of tableting materials. Eur. J. Pharm. Biopharm. **2000**, *49*, 267–273.
22. Picker, K.M.; Bikane, F. An evaluation of three-dimensional modeling of compaction cycles by analyzing the densification behavior of binary and ternary mixtures. Pharm. Dev. Technol. **2001**, *6*, 333–342.
23. Hersey, J.A.; Rees, J.E.; Cole, E.T. Density changes in lactose tablets. J. Pharm. Sci. **1973**, *62*, 2060.
24. Rees, J.E.; Rue, P.J. Time-dependent deformation of some direct compression excipients. J. Pharm. Pharmacol. **1978**, *30*, 601–607.
25. Ragnarsson, G.; Sjogren, J. Force displacement measurements in tableting. J. Pharm. Pharmacol. **1985**, *37*, 145–150.
26. Morris, L.E.; Moore, J.C.; Schwartz, J.B. Characterization and performance of a new direct compression excipient for chewable tablets: xylitab. Drug Dev. Ind. Pharm. **1996**, *22*, 925–932.
27. Eilbracht, M.; Steffens, K.J. Direct compression characteristics of a new form of granulated mannitol. Proc. 3rd World Meet. Pharm. Biopharm. Pharm. Technol. **2000**, *3*, 11–12.
28. Lerk, C.F. Consolidation and compaction of lactose. Drug Dev. Ind. Pharm. **1993**, *19*, 2359–2398.
29. Vromans, H.; de Boer, A.H.; Bolhuis, G.K.; Lerk, C.F.; Kussendrager, K.D.; Bosch, H. Studies on tableting properties of lactose. Part 2. Consolidation and compaction of different types of crystalline lactose. Pharm. Weekbl., Sci. **1985**, *7*, 186–193.
30. Picker, K.M.; Mielck, J.B. Effect of relative humidity during tabletting on matrix formation of hydrocolloids: densification behavior of cellulose ethers. Pharm. Dev. Technol. **1998**, *3*, 1–11.
31. Paronen, P.; Juslin, M. Compressional characteristics of four starches. J. Pharm. Pharmacol. **1983**, *35*, 627–635.
32. Bos, C.E.; Bolhuis, G.K.; van Doorne, H.; Lerk, C.F. Native starch in tablet formulations: properties on compaction. Pharm. Weekbl., Sci. Ed. **1987**, *9*, 274–282.
33. Steffens, K.J. A new maltodextrin as filler-binder for direct compression. Proc. 1st World Meet. Pharm. Biopharm. Pharm. Technol. **1995**, *1*, 143–144.
34. Bolhuis, G.K.; Chowhan, Z.T. Materials for direct compaction. In *Pharmaceutical Powder Compaction Technology*; Alderborn, G., Nyström, C., Eds.; Marcel Dekker Inc.: New York, 1996; 419–500.
35. Alderborn, G.; Nyström, C. Studies on the direct compression of tablets IV. The effect of particle size on the mechanical strength of tablets. Acta Pharm. Suec. **1982**, *19*, 190–381.